Title

A Systematic Comparison of Mathematical Models for Inherent Measurement of Ciliary Length: How a Cell Can Measure Length and Volume

Journal

Biophysical Journal, 108(6)

ISSN

0006-3495

Authors

Ludington, William B
Ishikawa, Hiroaki
Serebrenik, Yevgeniy V
et al.

Publication Date

2015-03-01

DOI

10.1016/j.bpj.2014.12.051

Peer reviewed

Article

A Systematic Comparison of Mathematical Models for Inherent Measurement of Ciliary Length: How a Cell Can Measure Length and Volume

William B. Ludington,[1] Hiroaki Ishikawa,[1] Yevgeniy V. Serebrenik,[1] Alex Ritter,[2] Rogelio A. Hernandez-Lopez,[2] Julia Gunzenhauser,[2] Elisa Kannegaard,[1] and Wallace F. Marshall[1,*]

[1]Department of Biophysics and Biochemistry, University of California, San Francisco, San Francisco, California; and [2]Physiology Course, Marine Biological Laboratory, Woods Hole, Massachusetts

ABSTRACT Cells control organelle size with great precision and accuracy to maintain optimal physiology, but the mechanisms by which they do so are largely unknown. Cilia and flagella are simple organelles in which a single measurement, length, can represent size. Maintenance of flagellar length requires an active transport process known as intraflagellar transport, and previous measurements suggest that a length-dependent feedback regulates intraflagellar transport. But the question remains: how is a length-dependent signal produced to regulate intraflagellar transport appropriately? Several conceptual models have been suggested, but testing these models quantitatively requires that they be cast in mathematical form. Here, we derive a set of mathematical models that represent the main broad classes of hypothetical size-control mechanisms currently under consideration. We use these models to predict the relation between length and intraflagellar transport, and then compare the predicted relations for each model with experimental data. We find that three models—an initial bolus formation model, an ion current model, and a diffusion-based model—show particularly good agreement with available experimental data. The initial bolus and ion current models give mathematically equivalent predictions for length control, but fluorescence recovery after photobleaching experiments rule out the initial bolus model, suggesting that either the ion current model or a diffusion-based model is more likely correct. The general biophysical principles of the ion current and diffusion-based models presented here to measure cilia and flagellar length can be generalized to measure any membrane-bound organelle volume, such as the nucleus and endoplasmic reticulum.

INTRODUCTION

Cells are bags of matter that somehow perform elaborate feats of organization. For example, cellular organelles are maintained in a precise size, shape, and position to optimize cellular physiology. Antibody-producing B cells have a greatly expanded endoplasmic reticulum, human sperm cells have a greatly expanded flagellum and precisely packed mitochondria, and plant parenchymal cells have a large central vacuole (1,2). In all of these cases, alteration in organelle size is a key feature of cellular architecture that relates to cellular function. However, the mechanisms by which cells control the size of organelles remain unknown in most cases.

The problem of size control for a cell is particularly interesting because an absolute measurement must be made without a standard ruler. Ask people how tall they are, and they will answer in calibrated units. However, every cell must make its own ruler from scratch, so the potential for variation is enormous. Several examples of cellular rulers have been described, including molecular ruler systems in bacteriophage tails, muscle thin-filament actin, and a measuring cup for bacterial flagellar hook growth (3). However, molecular rulers are not easily adaptable to changing circumstances, and for most organelles, the mechanisms that control size and shape remain unknown. Cilia and flagella serve as simplified model organelles for studying the more general question of organelle size control because their size can only vary in one dimension: length.

The eukaryotic cilium is a linear structure that projects out from the cell body. Eukaryotic cilia and flagella are compositionally equivalent, homologous organelles, with microtubules being the primary structural component. Assembly of the organelle occurs at the tip distal to the cell body. Precursor structural material is delivered to the tip through the action of intraflagellar transport (IFT) trains, which are complexes composed of microtubule motor proteins (kinesins and cytoplasmic dynein) and adaptor proteins, some of which bind ciliary precursor material (4–8). IFT trains enter the cilium through the ciliary pore, a membrane-spanning structure at the base of the cilium that may

Submitted November 5, 2014, and accepted for publication December 19, 2014.

*Correspondence: wmarshall@biochem.ucsf.edu

William B. Ludington's present address is Department of Molecular & Cell Biology, University of California, Berkeley, Berkeley, California.

Yevgeniy V. Serebrenik's present address is Department of Molecular, Cellular, and Developmental Biology, Yale University, New Haven, Connecticut.

Editor: David Odde.

0006-3495/15/03/1361/19 $2.00

http://dx.doi.org/10.1016/j.bpj.2014.12.051

be homologous to the nuclear pore (9,10), and certain proteins (e.g., kinesin II) must have a ciliary localization sequence to be admitted to the compartment. The basal body, a modified centriole, anchors the ciliary microtubules at the plasma membrane and integrates them with the cytoplasmic microtubules. The IFT proteins dock around this microtubule-organizing center and assemble into trains before entering the cilium (10). The amount of IFT traffic (i.e., the density of IFT trains on the cilium, equivalent to the rate at which trains enter the cilium (a.k.a. the flux)) and the rate at which flagellar precursor material is transported by these trains to the tip both appear to be regulated by the amount of material that is localized to the basal body: more material localizes in faster growing cilia, and individual cilia on a single cell can grow at different rates (6,11,12). Thus, correct ciliary length is achieved by regulating the accumulation of IFT material at the basal body and by the binding of ciliary precursor to IFT trains.

Although self-assembly establishes the organelle, a feedback system exists whereby the ciliary length dynamically regulates the assembly rate and disassembly rate (6,11,13–15). Thus, for this feedback to be established, the inherent mechanisms that control assembly and disassembly must somehow be tied to the ciliary length. Several distinct models have been proposed to establish a length dependence. Here, we derive quantitative, mathematical versions of these models and compare the predictions with published experimental data. The models we investigate are 1) no length dependence (i.e., the null model); 2) initial bolus of IFT protein (16,17); 3) time of flight (18); 4) ciliary current (19–22); 5) swim-speed feedback; 6) linear diffusion; and 7) volumetric diffusion (11). See Tables 1 and 2 for a summary.

The null model states that the ciliary length does not feed back on the assembly rate. Direct measurements conflict with this model (6,11,23); however, we include this model here as a null hypothesis.

The initial bolus model also does not require a length-dependent signal, but it is distinct from the null model. This model proposes that a precisely measured initial bolus of flagellar precursor material is set aside to build a flagellum, and no additional material is added (16,17). Thus, the cell makes a precise measurement at the beginning of ciliogenesis, but no dynamic feedback regulates the cilium once it is built. The bacterial flagellar length is set in such a manner.

The time-of-flight model (18) proposes that the cell directly measures length by tagging IFT trains entering the cilium with a degradable signal (e.g., a phosphorylation). The longer the cilium length, the greater is the amount of time spent by the signal molecule in the cilium, and the higher is the likelihood that the signal will revert to the ground state before exiting the flagellum. The length of the cilium can then be determined by the amount of excited-state signal molecules exiting the ciliary compartment. Several candidate signal molecules (e.g., small GTPases) exist in the cilium, but investigations have not shown them to be active length measurers. We derive a mathematical form of the time-of-flight model in the Results section.

Ciliary membrane ion channels can measure fluid flow and thus could provide a feedback on the length of the cilium (24,25). A longer cilium with more membrane channels would allow more current to pass, thus indicating length. In mammalian cells, bending by fluid flow has been shown to induce ciliary shortening through a calcium signal setting off a mitogen-activated protein kinase cascade (26), set off by a ciliary membrane mechanosensitive channel (27). Johnson and Rosenbaum (21) proposed that mechanosensitive membrane channels could represent a general model for ciliary length control (22,26).

The swim-speed feedback model proposes that *Chlamydomonas* changes its flagellar (i.e., ciliary) length to match the ideal length for swimming in its environment. The fluid coupling forces on a flagellum moving through a fluid will depend on the efficiency of the flagellar beating (28,29), which in turn depends on the flagellar length, the flagellar waveform (during beating), and the viscosity of the media (30,31).

A diffusion-based model for ciliary length control was first proposed by Levy (32). According to this model, if the tubulin dimers that form the cilium diffuse to the ciliary tip for assembly, the steady-state length can be set by limiting the supply of components that reach the tip, i.e., as the cilium grows longer, the increased distance to the cell body causes a lower tubulin concentration to be available. Since the discovery that IFT carries the structural components to the ciliary tip, this model appears less relevant. However, diffusion could still be relevant. Here, we propose two diffusion-based models based on the diffusion gradient of a signal molecule that is produced in the cilium and consumed in the cytoplasm. We call the first model the linear diffusion model because the signal is produced at the tip and sets up a linear gradient along the cilium. We call the second one the volumetric diffusion model because the diffusion gradient measures organelle volume.

We present the results in three parts. First, we derive formulations of the length-dependent signal for the 1) null hypothesis, 2) initial bolus of IFT protein (16,17), 3) time-of-flight (18), 4) ciliary current (19–22), 5) swim-speed feedback, 6) linear diffusion, and 7) volumetric diffusion (11) models. To translate the length-dependent signal into an empirical prediction for IFT regulation, we take into account the fixed number of potential binding sites for IFT proteins at the basal body and derive model solutions assuming that the length signals directly modulate IFT protein accumulation at the basal body. These derivations, using Langmuir binding, are presented in the "Placing the models in a ciliary length control context" subsection. We also use these model solutions to predict the total amount of IFT protein in the flagellum as a function of flagellar length. Finally, we present relevant empirical data that distinguish between several of the models. The ciliary

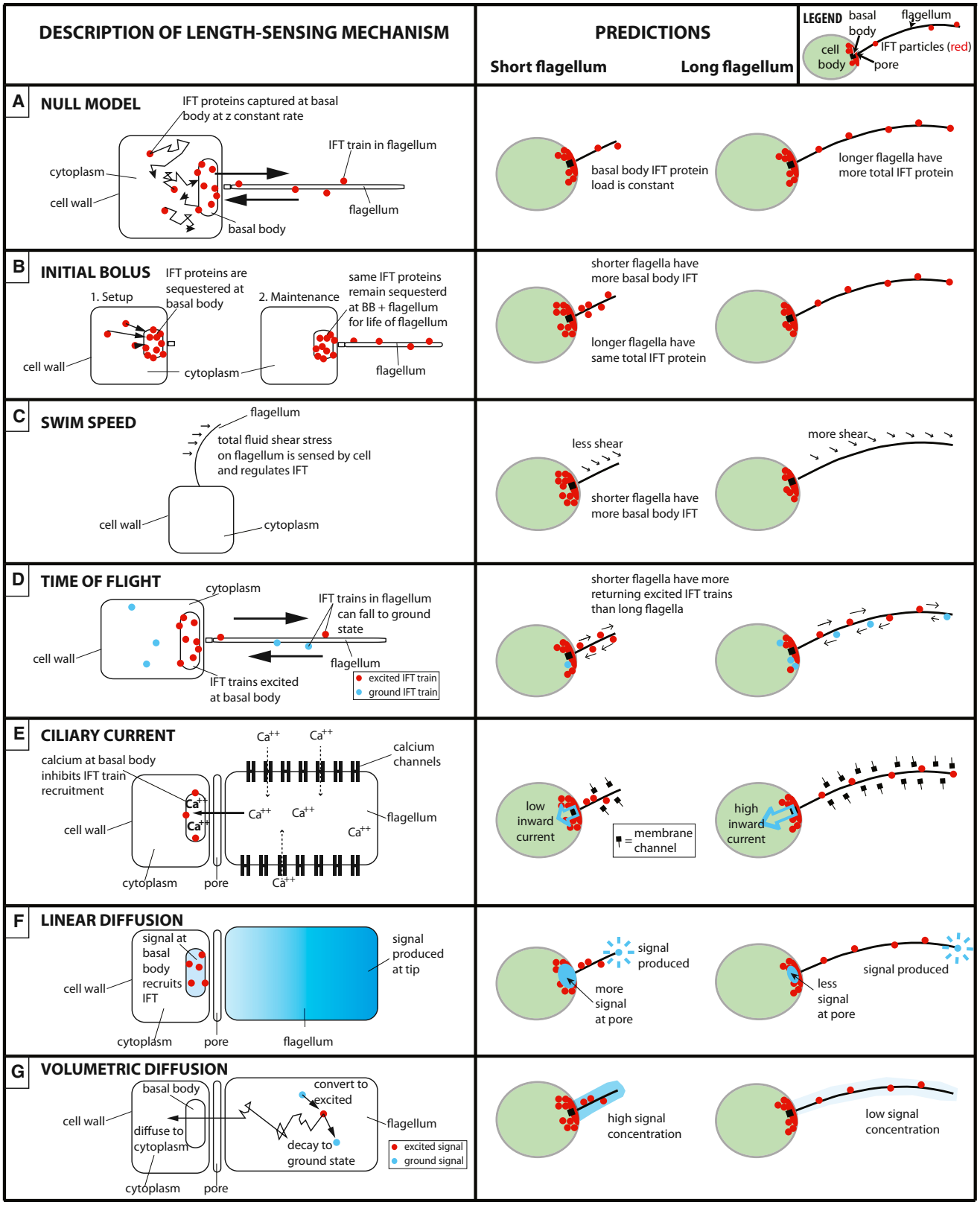

FIGURE 1 Schematics and predictions for each model. The models are described using a single flagellum on a *Chlamydomonas reinhardtii* cell as an example. The prediction for a cell with a short flagellum and a cell with a long flagellum is illustrated for each model. IFT trains are depicted as red dots. (*A*) The null model shows no regulation of IFT; that is, the frequency with which new IFT trains enter the flagellum is constant with respect to length because it only depends on the cytoplasmic concentration of IFT proteins, which is roughly constant. (*B*) The initial bolus model regulates IFT by assigning a

(legend continued on next page)

current model shows the best fit to data (our own as well as previous data). We discuss the models' agreement with data, further experiments that could be employed, and generalization of the biophysical principles to other membrane-bound organelle systems.

MATERIALS AND METHODS

Model simulations

All simulations and analyses were done in MATLAB (The MathWorks, Natick, MA). Model selection was performed using custom-written code. The corrected Akaike information criterion (AIC_C) (33,34) was used for model selection and is calculated as

$$AIC_C = n \ln\frac{RSS}{n} + \frac{2nk}{n-k-1}, \quad (1)$$

where $\boldsymbol{n}$ is the number of sample data points (here, $n = 186$ IFT KAP-GFP injection rate versus flagellar length data points or $n = 317$ basal body concentration of KAP-GFP IFT proteins versus flagellar length data points), $\boldsymbol{RSS}$ is the residual sum of squares calculated between the model prediction and the sample data points, and $\boldsymbol{k}$ is the number of fitted parameters for each model.

IFT rate measurements

All measurements were performed as previously described (11). Briefly, *Chlamydomonas* KAP-GFP ΔKAP cells (a generous gift from Mary Porter, University of Minnesota) express a GFP tag on the KAP (*fla3*$^-$) subunit of the flagellar kinesin II motor protein, which is a part of every IFT complex that enters the cilium. KAP-GFP cells were grown in M1 minimal media and deflagellated by pH shock at pH 4.6 for 2 min. Cells were washed in fresh M1 and transferred to a poly-L-lysine-treated coverslip on a Nikon Instruments (Melville, NY) ti2000 total internal reflection fluorescence (TIRF) microscope with a calibrated illumination field (488 nm excitation, 525 nm emission). As the cells regenerated their flagella, they were imaged. Kymographs were constructed and analyzed using custom scripts in MATLAB to detect KAP-GFP in the flagella (35). Measurements were made of the IFT intensity, speed, and frequency.

Fluorescence recovery after photobleaching experiments

Fluorescence recovery after photobleaching (FRAP) experiments were conducted on a Nikon ti2000 custom fitted by Andor Technology (Belfast, UK) with a Yokogawa Electric Corporation (Tokyo, Japan) CSU22 spinning-disk confocal and a separate bypassing FRAP laser. The laser launch and microscope software were custom Andor products used in the Woods Hole Physiology Course (Marine Biological Laboratories, Woods Hole, MA) in 2009. Further experiments employed a Zeiss spinning-disk Axio Observer.Z1 equipped with a UGA-40 FRAP module. Images were acquired with an exposure time of 100 ms. The *Chlamydomonas reinhardtii* strains used were the above-mentioned KAP-GFP ΔKAP (36) and an IFT20-GFP rescue of an IFT20Δ strain (37). IFT20 is another protein component of IFT complexes. Cells were grown and imaged in standard liquid Tris-acetate-phosphate (TAP; rich) media. Cells were trapped in a CellASIC (San Leandro, CA) microfluidic chamber, one flagellum was bleached using a continuous pulse of 405 nm laser light, and the fluorescence recovery was recorded over time. Alternately, cells were trapped under a slab of 0.5% agarose prepared in TAP media.

Flagellar length measurement

Cell lines were obtained from the Chlamydomonas Resource Center (St. Paul, MN). Cells were grown in liquid TAP rich media and fixed in glutaraldehyde before light micrographs were obtained through a 40× lens on a Zeiss (Oberkochen, Germany) microscope. Length was quantified using hand traces of flagella in ImageJ.

Beat frequency versus flagellar length

CC125 (wild-type) and *lf1* (mutant with abnormally long flagella) strains were obtained from the Chlamydomonas Stock Center. Cells were grown in liquid TAP rich media and imaged on a Zeiss Axiovert 200M with a 40× lens and a Phantom MiroEX4-1024 MM high-speed camera running at 1000 fps under IR filtered light with a 998 μs exposure time.

RESULTS

Previous studies have shown that eukaryotic cilia and flagella are dynamic structures that undergo constant turnover (16). Our goal was to understand how inherent length-dependent signals produced by these organelles could lead to stable steady-state length.

Null model

The simplest model is that the IFT rate is not regulated by ciliary length at all (Fig. 1 *A*). Thus, the rate at which ciliary precursor material is transported to the tip for assembly is solely dependent on the concentration of IFT material in the cytoplasm, which under a null model is not regulated in response to length (e.g., in contrast to previous studies (38,39)). The signal as a function of flagellar length, $\boldsymbol{S_{NM}(L)}$, is simply a constant (Table 1; Fig. 2 *A*):

$$S_{NM}(L) = k. \quad (2)$$

Many lines of empirical data dispute this model. The *Chlamydomonas* flagellar proteome and transcriptome (38,39), the IFT rate (11), the amount of IFT material

set number of IFT trains to each flagellum when they are first initialized. These IFT proteins are in a closed pool that never exchanges with the cytoplasmic pool of IFT proteins. (*C*) The swim-speed feedback model postulates that length is sensed by a mechanosensory feedback due to channels on the flagellar membrane being stretched by the coupling force with the extracellular fluid. (*D*) The time-of-flight model proposes that a signal molecule attached to each IFT train that enters the flagellum measures the length because IFT trains stay longer in long flagella and thus have a higher probability of the signal molecule falling to the unexcited state. (*E*) The ciliary current model proposes that ion channels on the flagellar membrane regulate length by allowing a current to pass into the cell body. Longer flagella, which have more channels, let in a larger current. (*F*) The linear diffusion model suggests that the flagellar base senses a signal produced at the flagellar tip. The longer the flagellum, the lower is the signal sensed by the base. (*G*) The volumetric diffusion model extends the linear diffusion model such that signal is produced throughout the flagellum at a constant rate and can either decay in the flagellum or escape into the cytoplasm. The concentration of signal in the flagellar compartment decreases as the flagellar compartment becomes larger. To see this figure in color, go online.

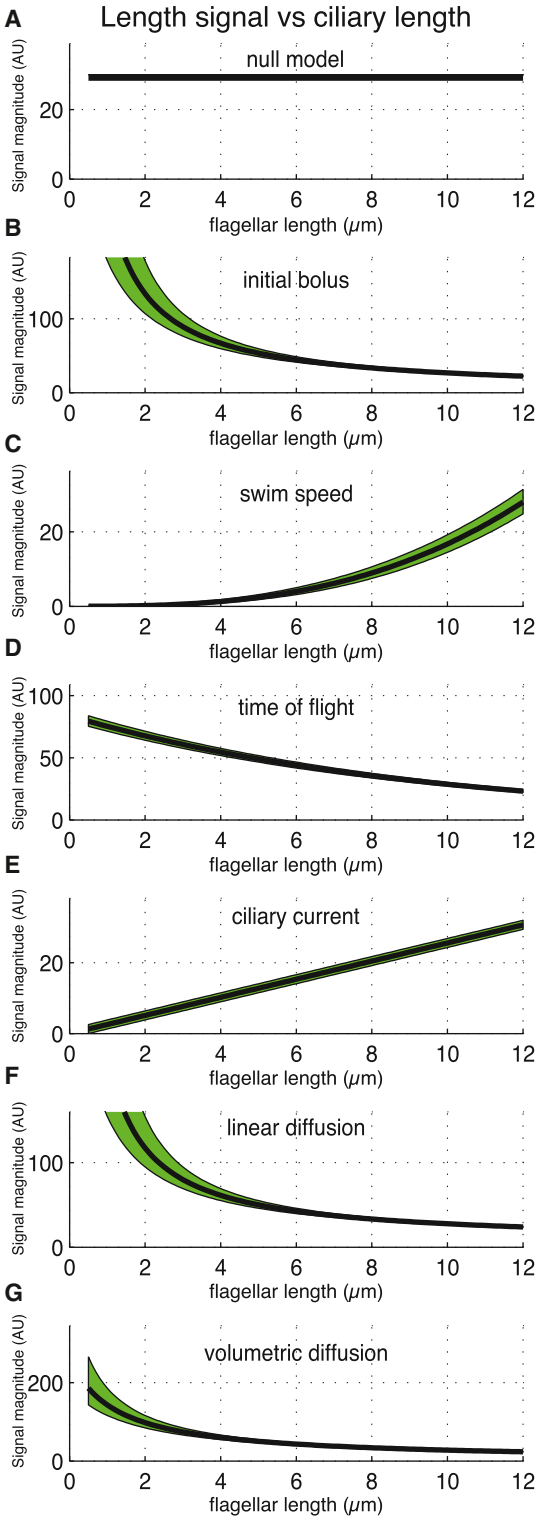

FIGURE 2 Many length-measuring signals can exist in the cell. The length-measuring signal for each model (*A*, null; *B*, initial bolus; *C*, swim speed; *D*, time of flight; *E*, ciliary current; *F*, linear diffusion; *G*, volumetric diffusion) is plotted as a function of flagellar length (*black lines*). To show how sensitive each length signal is to small mismeasurements of length, the green shaded region shows how the signal changes if the sensed length is $\pm 0.5\ \mu$m. The *y* axis scale differs among the models because they were fit to an IFT versus length data set (see Fig. 6). To see this figure in color, go online.

that is docked at the basal bodies (11,40), and the cargo-loading rate (6) have all been shown to be length dependent, and stable flagellar length may also be achieved through active regulation of disassembly (15). These diverse data strongly suggest that ciliary length feeds back on the regulation of assembly and disassembly, but we first consider one additional model in which active length sensing is not explicitly required: the so-called initial bolus model.

Initial bolus model

The initial bolus model proposes that the cell allocates a fixed amount of IFT machinery to each cilium as an initial bolus when the cilium begins to assemble, analogously to how a bacterial flagellar hook is formed (16,17,41) (Fig. 1 *B*). The cell must still make a measurement to determine the size of the initial bolus, but after the initial bolus is formed, IFT proteins neither enter nor leave that pool of proteins associated with that single cilium.

Marshall and Rosenbaum (16) and Marshall et al. (17) first proposed this model to account for the roughly constant amount of IFT protein in a *Chlamydomonas* flagellum as a function of length. They showed that under this assumption, the IFT rate as a function of ciliary length, $\boldsymbol{L}$, is

$$S_{IB}(L) \propto \frac{1}{L}. \tag{3}$$

Thus, the IFT rate is higher in a short cilium than in a long cilium because the same number of trains are spread out over a longer distance in the long cilium. Since the IFT trains continuously move between the tip and base in this model, an inherent measurement of length is established by the frequency with which the trains arrive at the tip or base (Fig. 2 *B*).

Swim-speed model

Another inherent length signal could be produced by ions leaking though the ciliary membrane as a result of membrane stretching due to viscous coupling forces with the fluid. As the cilia push through viscous fluid, they experience a coupling force on their membrane (31) (Fig. 1 *C*). At the low Reynolds number of ciliary beating (~10^{-3}), viscous forces dominate over inertia, and fluid motion can be approximated with Stokes equations of motion (30). By treating a cilium as a very thin ellipsoid, Harris (31) used the derivation by Jeffery (42) for an ellipsoidal particle moving through viscous fluid to approximate the coupling force, $\boldsymbol{C_x}$, between a cilium of length, $\boldsymbol{L}$, and the fluid during the effective stroke (i.e., not for the recovery stroke, which is less):

$$C_x = \frac{4\pi}{3\ln(20L)}\mu L^3\omega, \tag{4}$$

where $\boldsymbol{\mu}$ is the fluid viscosity and $\boldsymbol{\omega}$ is the angular velocity of the ciliary beat. If we assume that the cell senses this force (e.g., due to ions leaking through stretched membrane channels), then there exists a length signal, $S_{SS}(L) \propto C_x$, that is proportional to the viscosity and beat speed as well as roughly the cube of length (Fig. 2 *C*). The length-dependent signal is not the force directly, but rather could be sensed by the cell as the flux of ions through the ciliary compartment into the cell body, where active ion pumps maintain a constant ion concentration (22). Because no details of such a system are explicitly known, we propose that the length-dependent signal inhibits IFT train accumulation at the basal body (see "Placing the models in a ciliary length control context" below).

Time-of-flight model

The time-of-flight model proposes that the amount of time an IFT protein spends in the ciliary compartment inherently measures the length of the organelle (18). Because IFT proteins are transported out to the tip and back to the base of the cilium at a roughly constant speeds, the total time an IFT protein spends in the cilium from the time it enters the cilium until the time it reemerges back into the cytoplasm will be longer for longer cilia (Fig. 1 *D*). To formulate this scenario into a simple quantitative model, we propose that IFT trains are modified with a signal before they enter the cilium, and that while they are inside the cilium, they lose the modification at a constant rate. The modification could be any transient protein modification, such as a phosphorylation or a protein-protein binding event, such that the modified form can degrade to the unmodified form. To specify a mathematical prediction of this length sensor, we make the following assumptions.

1. IFT trains in the excited state, $\boldsymbol{S}^*$, are injected into the cilium.
2. While traveling inside the cilium, signal in the $\boldsymbol{S}^*$ form degrades to $\boldsymbol{S}$ with first-order kinetics, $S^* \xrightarrow{k} S$.
3. IFT velocity is approximately constant along the cilium length, hence the time an IFT train spends in the cilium, $\boldsymbol{t}$, is proportional to the cilium length divided by the harmonic mean of the anterograde and retrograde speeds, $\boldsymbol{v}$, plus the time spent at the tip, $\boldsymbol{t_T}$, or equivalently, $t(L) = 2L/v + t_T$.
4. The signal is sensed at ejection from the cilium as the amount of S^* at the basal body.

Therefore, $dS^*/dt = -kS^*$, and $\ln(S^*) = -kt + D_0$, or

$$S^*(t) = De^{-kt}, \tag{5}$$

where $D = e^{D_0}$ is a constant. Reformulating $S^*(t)$ as a function of length, we have

$$S_{TF}(L) = De^{-k\left(\frac{2L}{v}+t_T\right)}. \tag{6}$$

Thus, the proportion of modified IFT trains exiting the cilium will decrease exponentially with flagellar length (Fig. 2 *D*).

Our own measurements of IFT velocities show that they are not constant as a function of length, but rather the velocities are slower in shorter flagella (43), where the IFT trains are more crowded. Although this length dependence of v is not a large effect, it does make the decay of the exponential shallower, decreasing the length dependence of the IFT injection rate.

A factor in the reliability of the time-of-flight length sensor is the amount of IFT traffic in the cilium. If IFT is shut down, the sensor does not work, and when IFT is very low, the sensor becomes noisy. Likewise, if IFT is impaired by crowding, as may occur in extremely short regenerating cilia, the sensor reads out a longer than actual length. However, low IFT occurs in longer cilia, where the signal is low anyway, and regenerating short cilia may already be operating at maximum IFT rate, so functional problems for such a sensor may be unimportant in terms of maintaining proper ciliary length.

As a mechanism of sensing this length signal, we propose that exiting IFT trains in the excited state preferentially rebind the basal body due their locally higher concentration (i.e., in addition to the normal binding of IFT trains from the cytoplasmic pool).

Ciliary current model

Cilia have membrane calcium channels, and bending by fluid flows can induce a current that causes ciliary shortening (19,24–26,44,45). Rosenbaum (20) and Johnson and Rosenbaum (21) proposed that this current could provide a mechanism of ciliary length sensing. Further evidence indicates that calcium currents may play a role in ciliary length. For example, changing the tonicity of the growth medium for *Chlamydomonas* can increase or decrease ciliary length significantly (46–48), and length is also sensitive to internal and external calcium concentrations (49). The basic premise for this model is that ion channels in the ciliary membrane produce a current through the ciliary pore that serves as the length signal (20–22), $\boldsymbol{S(L)}$ (Fig. 1 *E*). To derive $S(L)$, we make the following assumptions.

1. Voltage-dependent calcium channels occur at constant density on the cilium surface (i.e., there are more ion channels in a longer flagellum (22)), independently of flagellar length, $\boldsymbol{L}$, and act as resistors to current flow across the flagellar membrane. Such a constant density of channels could be maintained on the cilium if the channels occur on the cell membrane at constant density and can freely exchange with the ciliary membrane.
2. The cell maintains a constant voltage, $\boldsymbol{V_{cell}}$, on the cell body through the action of ion pumps (22).

3. A calcium current passes from the cilium into the cell body through the ciliary pore based on the difference in potential between the cell body and the cilium.
4. All of the ciliary channels have the same resistance and the probability of a channel being open is fixed, independently of the number of channels. Thus, the current is proportional to the number of channels.
5. $V_{cilium} = IR_c$, i.e., we assume that the product of the current, $\boldsymbol{I}$, and the ciliary resistance, $\boldsymbol{R_c}$, equals the voltage across the ciliary membrane according to Ohm's law.
6. The ciliary resistance can be attributed to the open channels.

The cilium's resistance is calculated as

$$\frac{1}{R_c} = \sum_{i=1}^{n} \frac{1}{R_i} \tag{7}$$

or equivalently n/R_i, where $\boldsymbol{n}$ is the number of open channels on the flagellum, and $\boldsymbol{R_i}$ is the resistance of a single open channel. Because we assume that $\boldsymbol{n}$ is proportional to the flagellar length due to a constant channel density and a constant likelihood of being open,

$$I_{pore} = \frac{nV_{cell}}{R_i}. \tag{8}$$

Because $\boldsymbol{V_{cell}}$ and $\boldsymbol{R_i}$ are constants and $\boldsymbol{n}$ is proportional to the ciliary length,

$$I_{pore} \propto L. \tag{9}$$

Thus, $S_{CC}(L) \propto L$, so the ciliary current could serve as an excellent length sensor. Rosenbaum (20) proposed that the current could modify a biochemical pathway that regulates IFT. To place the sensor in the context of a length-control system, we propose that ciliary calcium influx at the basal body could inhibit cargo binding by IFT trains, as per Wren et al. (6), or IFT protein docking at the basal body (Fig. 3 *B*) (11). Thus, the model predicts that the number of IFT trains at the basal body will be greater when the intracellular calcium is lowered, and that the steady-state ciliary length should increase under these conditions (Fig. 2 *E*). The ciliary length result has already been demonstrated by Besschetnova et al. (26). Furthermore, while this manuscript was in review, Liang et al. (14) published results from a genetic-mechanism study in *Chlamydomonas* demonstrating that calcium induces phosphorylation of kinesin-II to prevent its entry into the cilium, which is entirely consistent with the ciliary current model.

Linear diffusion gradient

Diffusion is a fundamental process that affects many aspects of life. In the context of organelle size control, diffusion has been shown to set up the Ran-GTP gradient that regulates both bipolar spindle formation during cell division and nuclear import and export during the rest of the cell cycle (50–52). Here, we present diffusion as a method for the cell to measure cilium length. This model is based on the idea that a signal emitted from the cilium tip and received at the ciliary pore will produce a higher signal when the emitter is closer to the receiver (i.e., short cilium) and a lower signal when the distance is greater (i.e., long cilium) (Fig. 1 *F*).

We make the following assumptions.

1. The concentration of the signal molecule (e.g., a structural component of the cilium, such as the outer dynein arm protein) at the ciliary tip remains constant due to equilibrium binding with the tip (see Supporting Material). We call this constant concentration $\boldsymbol{C_{tip}}$.
2. The cytoplasm contains a sink for the signal molecule so that the concentration is a constant, $\boldsymbol{C_{cyto}}$.
3. The signal sensor sits a distance, $\boldsymbol{b}$, toward the tip from the cytoplasmic sink (e.g., in the ciliary pore).
4. Normal diffusion occurs.
5. The system reaches steady state much faster than the length changes (32).
6. We can approximate the cilium as a linear structure.

For diffusion, the concentration, $\boldsymbol{C}$, changes with time along the length of the cilium, $\boldsymbol{x}$. Thus, according to Fick's second law,

$$\frac{\partial C(x,t)}{\partial t} = D \cdot \nabla^2 C(x,t). \tag{10}$$

Solving for the concentration a distance x from the tip of the cilium at steady state,

$$C(x) = \frac{A_1}{D}x + \frac{A_2}{D}. \tag{11}$$

We use boundary conditions, $C(x=0) = C_{tip}$ and $C(x=L) = C_{cyt}$, where L is the total length of the cilium, D is the diffusion constant, and A_1 and A_2 are constants of integration. We define a one-dimensional coordinate system to have an origin with $x = 0$ at the tip. Thus,

$$C(x) = C_{tip} - \frac{C_{tip} - C_{cyto}}{L}x. \tag{12}$$

The function gives the concentration anywhere along the length of the cilium, a length, x, from the tip. We have defined the ciliary pore as the site where the length signal is measured, so setting $x = L - b$ and simplifying, we have

$$C_b(L) = C_{cyto} + b\frac{C_{tip} - C_{cyto}}{L}. \tag{13}$$

Thus, the length signal at the pore as a function of cilium length is

$$S_{LD}(L) = C_{cyto} + b\frac{C_{tip} - C_{cyto}}{L}. \tag{14}$$

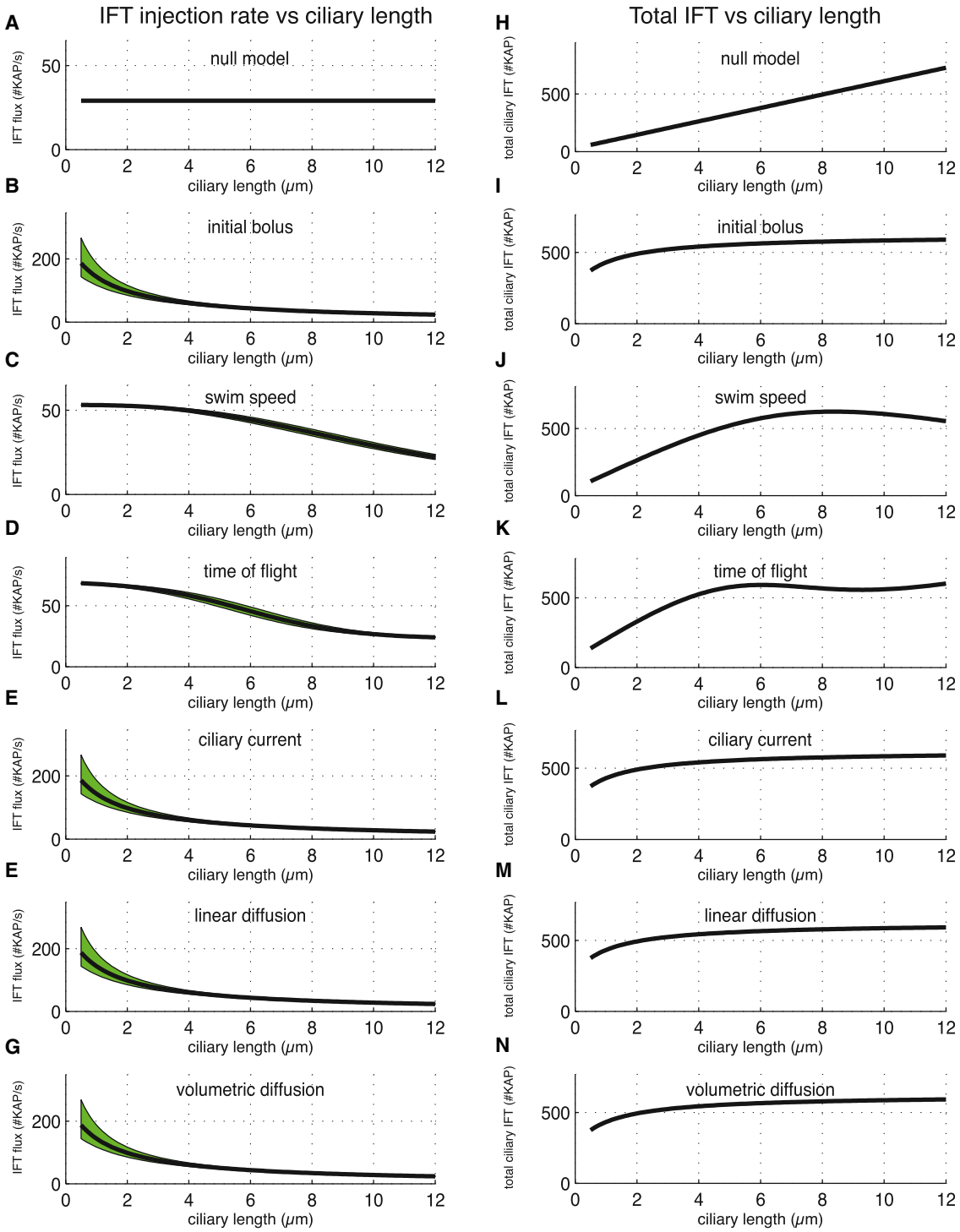

FIGURE 3 (*A–N*) Model predictions for the IFT protein flux into the cilium (*A–G*) and the total ciliary IFT protein (*H–N*). The equations in Table 1 were fit to IFT injection data (11). To depict how sensitive each length model is to small mismeasurements of length, the green shaded region shows how the model outputs changes if the sensed length is ± 0.5 μm. (*H–N*) Model predictions for the total ciliary IFT protein versus ciliary length were calculated using the parameter fits from (*A*)–(*G*). To see this figure in color, go online.

Volumetric diffusion model

Because most organelles are not linear structures, but rather can be quite convoluted (e.g., the endoplasmic reticulum), the cell needs a way to measure volume. We propose volumetric diffusion as an internally consistent and robust way for a cell to measure the size of any membrane-bound

organelle or even the cytoplasmic fraction of the cell itself (Fig. 1 *G*). We previously proposed the volumetric diffusion model to explain empirical data indicating that IFT proteins accumulate at the basal body as a function of cilium length (11), and that a RanGTP gradient regulates IFT protein entry into the ciliary compartment much as the gradient regulates nuclear import of nuclear proteins (9). Here, we rederive the model for the general case, in which the signal molecule is unknown. We make the following assumptions.

1. As in the time-of-flight model, volumetric diffusion requires a signal molecule that can switch from an excited state to a ground state (e.g., Ran).
2. The signal molecule is produced at a constant rate within the flagellum (i.e., a constant number of molecules per unit of time) due to the constant activity of the enzyme that produces it.
3. The precursor to the signal molecule occurs in a constant, saturating amount inside the ciliary compartment.
4. The gradient of the signal molecule across the ciliary pore reaches steady state much faster than the ciliary length changes.
5. No spatial gradient of signal molecule exists within the ciliary compartment because the compartment is well mixed (e.g., by the movement of the cilium and IFT trains within it). Note that assumptions 3 and 4 together let us assume a steady state for the signal molecule.
6. The signal molecule decays at a constant rate according to first-order kinetics, with no effect of length on the hydrolysis rate.
7. The signal molecule concentration in the cytoplasm is very small compared with the ciliary concentration.
8. The signal molecule diffuses from the cilium according to Fick's first law, $J = -D(\partial\phi/\partial x)$, where J is the diffusive flux, ϕ is the ciliary concentration, and x is the pore length. Thus, the diffusive loss is the flux, J, times the cross-sectional area, a.
9. The cilium shape can be approximated by a cylinder.

With these assumptions, we calculate the rate of change of the number of signal molecules in the ciliary compartment,

$$\frac{dN}{dt} = k_{prod} - k_{cat}N - \frac{k_{esc}N}{L}, \tag{15}$$

where N is the number of signal molecules in the cilium, k_{prod} is the production rate of new signal molecules, k_{cat} is the decay rate (inverse of the half-life), L is the cilium length, and k_{esc} is a proportionality constant that takes into account the diffusion constant and the length of the flagellar pore ($k_{esc} = D/l$, where D is the diffusion constant and l is the pore length).

Thus, a signal molecule in the cilium can either diffuse to the cytoplasm or decay within the cilium (see Fig. 1). The steady-state solution for the number of signal molecules, N^*, is

$$N^* = \frac{k_{prod}L}{k_{cat}L + k_{esc}}, \tag{17}$$

Thus, as the length increases, the number of signal molecules in the excited state reaches a limit. However, the concentration of excited-state molecules in the ciliary compartment is proportional to N^*/L, which we see decreases as the ciliary compartment grows in size (Fig. 2 *G*):

$$S_{VD}(L) = \frac{k_{prod}}{k_{cat}L + k_{esc}}. \tag{18}$$

Thus, volumetric diffusion can provide an inherent volume sensor for the cell because the probability that an excited molecule will diffuse out of the cilium before it hydrolyzes becomes smaller as the ciliary compartment becomes larger. Because both IFT train localization to the basal body and IFT train cargo loading appear to be regulated by the ciliary length sensor, an obvious test of this model would be to artificially swell a short, regenerating cilium and measure how basal body localization and cargo loading are affected. A swollen cilium with larger volume should reach steady-state length at a shorter length than would an unswollen cilium.

Applying the model specifically to the case of a RanGTP gradient, we previously demonstrated that the parameters of the model agree well with published values measured independently (11).

Placing the models in a ciliary length-control context

The model solutions that we calculated in the preceding sections solve for length signal, $S_{XX}(L)$, to which a cell may respond. Other investigators and we have empirically measured this cellular response in terms of IFT regulation as a function of flagellar length (6,11,14,23,43,53,54), i.e., $I_{XX}(L)$ in Table 1. To place the model solutions for the length signal in the context of ciliary length control, we must formulate a mechanism by which the length signal, $S_{XX}(L)$, can be translated into IFT regulation, $I_{XX}(L)$. Here, we propose that the length signal acts at the basal body to regulate IFT accumulation and cargo loading. Therefore, we take into account that a limited number of docking sites exist at the basal body where IFT trains can bind.

We use an analog of Langmuir binding for a molecule in solution binding to limited sites on a solid substrate to approximate saturation of the basal body docking sites for IFT-related proteins ($IFT_{cyto} + BB_{free} \rightleftharpoons IFT_{BB}$, where $\boldsymbol{IFT_{cyto}}$ is IFT protein in the cytoplasm that can bind free basal body sites, $\boldsymbol{BB_{free}}$). Thus, the concentration of adsorbed IFT material on the surface of the basal body, $[\boldsymbol{IFT_{BB}}]$, has the form

$$[IFT_{BB}] = \frac{K_{eq}[IFT_{cyto}]}{K_{eq}[IFT_{cyto}] + 1}[IFT_{max}], \tag{19}$$

where $[\boldsymbol{IFT_{max}}]$ is the concentration when all IFT train recruitment sites on the basal body are occupied, and $\boldsymbol{K_{eq}}$ is the equilibrium fraction ($K_{eq} = k_{ad}/k_d$) when the rate of adsorption, $r_{ad} = k_{ad}IFT_{cyto}BB_{free}$, equals the rate of desorption, $r_d = k_dIFT_{BB}$.

The different assumptions in the initial derivations of the length sensors require slightly different formulations of the basal body binding model. The final equations for $I_{XX}(L)$ (with lumped parameters; see Table S1) are shown in Table 1 and plotted in Fig. 3, *A–G*. Here, we briefly describe the specific formulation of each solution for $I_{XX}(L)$. For the null model, $[IFT_{BB}]$ is just a constant because K_{eq}, IFT_{cyto}, and IFT_{max} are all constants in this case. For the initial bolus model, we assume that the length signal directly produces the concentration of material available to bind the basal body, IFT_{cyto}. For the swim-speed and ciliary current models, we assume that the ion current produced in these models directly modulates the disassociation constant, k_d, making IFT trains dissociate more readily from the basal body as the cilium gets longer (i.e., the current gets larger). For the time-of-flight model, we propose that the returning IFT trains in the excited state can directly rebind the basal body, making the local concentration of IFT material higher at the basal body. In this case, $[IFT_{cyto}]$ is the sum of the constant cytoplasmic concentration of IFT proteins plus the concentration of returning IFT trains in the excited state. Finally, for the diffusion models, we assume that the length signal directly modulates the adsorption rate constant, k_{ad}. Thus K_{eq} increases for shorter cilia.

By considering the saturation of IFT binding at the basal body, we get the solutions, $I_{XX}(L)$, of the models presented in Table 1. The effect of saturation is to decrease the sensitivity of the length signal (i.e. $\Delta S/\Delta L$) at short lengths. The effect is most pronounced for the initial bolus model and the linear diffusion model, which are hyperbolic (Table 1). Thus, these models no longer go to infinity at zero length.

We have derived the predictions for the basal body accumulation of IFT material, and we further assume that the rate of material entering the cilium (i.e., the flux into the cilium) is directly proportional to the amount of material accumulated at the basal body. This assumption appears justified based on published data (6,11,40)

Notably, the equations for the initial bolus and ciliary ion current models are equivalent under the Langmuir binding assumptions. Thus, while providing an equivalent mathematical form, the ciliary ion current model provides a mechanism that is distinct from the initial bolus for the maintenance of a constant IFT protein pool in the cilium, as proposed in Marshall and Rosenbaum (16) and Marshall et al.'s (17) original balance point model, because it allows turnover of IFT proteins.

We also note that the diffusion models become algebraically equivalent to the ciliary current and initial bolus models when the respective k_2 constants from the diffusion models go to the limit of zero. For the linear diffusion model, k_2 is the cytoplasmic concentration of signal molecule, which does not seem an unreasonable assumption. For the volumetric diffusion model, k_2 is the escape parameter, requiring either the diffusion constant through the pore to be zero or the pore length to be infinite. Setting up the cilium as a completely sealed chamber may be a reasonable assumption for some proteins.

Calculation of the total ciliary protein as a function of length

Another IFT parameter that has been empirically measured is the total amount of IFT trains in a flagellum as a function of length (16,17), i.e., $T_{XX}(L)$ in Table 1. Therefore, we use the fitted models to predict the total amount of IFT protein in the cilium as a function of ciliary length by integrating the amount of IFT material over the round-trip journey for an IFT protein inside the flagellum (Fig. 3, *H–N*),

$$IFT_{tot} = k_{in}IFT_{BB}\left(\frac{2L}{v} + t_T\right), \tag{20}$$

where the time spent in the flagellum is as calculated in Eq. 6. Note that in Eq. 19, we calculate the concentration of protein at the basal body, but since the basal body volume is constant, IFT_{BB}, the total amount of IFT protein accumulated at the basal body, is proportional to $[IFT_{BB}]$, the IFT protein concentration on the basal body. This equation allows us to calculate the predicted total flagellar IFT protein as a function of length for each model, yielding $T_{XX}(L)$ (Table 1). k_{in} is a rate constant specifying what proportion of the IFT material that has accumulated at the basal body, IFT_{BB}, is injected into the flagellum per second; L is the flagellar length; v is the harmonic mean of the anterograde and retrograde IFT speeds; and t_T is the dwell time at the flagellar tip before the retrograde journey begins. As shown in Fig. 3, with the exception of the null model, the various models all reach a plateau for the total ciliary IFT material, but they reach the plateau at different ciliary lengths and with different steepness of approach. Published data show that the total amount of IFT protein is roughly constant in *Chlamydomonas* flagella from 1 μm up to 12 μm (16,17). The constant-injection, swim-speed, and time-of-flight models do a poor job of replicating that observation, but the other models replicate it well.

Weak empirical support for the swim-speed model

Clearly, the swim-speed model only applies to motile cilia that are actively moving. However, it makes three easily testable predictions: 1) increasing viscosity will cause the cilia to either shorten by a small amount or decrease their angular velocity in proportion to the increase in viscosity, 2) paralyzed

TABLE 1 Summary of the model equations

Models	Length signal versus length	IFT versus length	Total IFT protein versus length	Length-measuring mechanism
Null model	$S_{NM}(L) = k_1$	$I_{NM}(L) = k_1$	$T_{NM}(L) = k_1\left(\frac{2L}{v} + t_T\right)$	none
Initial bolus	$S_{IB} = \frac{k_1}{L}$	$I_{IB}(L) = \frac{k_1/L}{k_1/L + 1}k_2$	$T_{IB}(L) = \frac{k_1\left(\frac{2L}{v} + t_T\right)/L}{k_1/L + 1}k_2$	frequency of IFT or amount of IFT protein at basal body
Swim speed	$S_{SS}(L) = \frac{k_1L^3}{\ln(20L)}$	$I_{SS}(L) = \frac{k_2\ln(20L)/k_1L^3}{k_2\ln(20L)/k_1L^3 + 1}k_3$	$T_{SS}(L) = \frac{k_2\ln(20L)\left(\frac{2L}{v} + t_T\right)/k_1L^3}{k_2\ln(20L)/k_1L^3 + 1}k_3$	coupling force between the cilium and extracellular media
Ciliary current	$S_{CC} = k_1L$	$I_{CC}(L) = \frac{k_1/L}{k_1/L + 1}k_2$	$T_{CC}(L) = \frac{k_1\left(\frac{2L}{v} + t_T\right)/L}{k_1/L + 1}k_2$	ion flow across the ciliary pore
Time of flight	$S_{TF}(L) = k_1e^{-k_2\left(\frac{2L}{v} + t_T\right)}$	$I_{TF}(L) = \frac{k_1e^{-k_2\left(\frac{2L}{v} + t_T\right)} + k_3}{k_1e^{-k_2\left(\frac{2L}{v} + t_T\right)} + k_3 + 1}k_4$	$T_{TF}(L) = \frac{\left(k_1e^{-k_2\left(\frac{2L}{v} + t_T\right)} + k_3\right)\left(\frac{2L}{v} + t_T\right)}{k_1e^{-k_2\left(\frac{2L}{v} + t_T\right)} + k_3 + 1}k_4$	excitation state of signal molecules leaving the ciliary compartment
Linear diffusion	$S_{LD}(L) = \frac{k_1}{L} + k_2$	$I_{LD}(L) = \frac{k_3\left(\frac{k_1}{L} + k_2\right)}{k_3\left(\frac{k_1}{L} + k_2\right) + 1}k_4$	$T_{LD}(L) = \frac{k_3\left(\frac{k_1}{L} + k_2\right)\left(\frac{2L}{v} + t_T\right)}{k_3\left(\frac{k_1}{L} + k_2\right) + 1}k_4$	slope of the diffusion gradient
Volumetric diffusion	$S_{VD}(L) = \frac{k_1}{k_2 + L}$	$I_{VD}(L) = \frac{k_3\left(\frac{k_1}{k_2 + L}\right)}{k_3\left(\frac{k_1}{k_2 + L}\right) + 1}k_4$	$T_{VD}(L) = \frac{k_3\left(\frac{k_1}{k_2 + L}\right)\left(\frac{2L}{v} + t_T\right)}{k_3\left(\frac{k_1}{k_2 + L}\right) + 1}k_4$	concentration gradient between the cilium and cytoplasm

Mathematical formulations of the model solutions are summarized here. To emphasize the form of the equations, the free parameters have been lumped into the constants, k_i, that are fit to data (see Figs. 2, 3, and 6). The length signal equations, $S_{XX}(L)$, describe the length dependence of the biophysical processes modeled. IFT versus length, $I_{XX}(L)$, describes how the process would regulate IFT. The derivation (Eq. 19) takes into account the signal strength as well as the limited number of binding sites for IFT proteins at the basal body. Total IFT protein versus length, $T_{XX}(L)$, describes how the total amount of IFT protein in the cilium varies with ciliary length by taking into account the time that the IFT proteins spend inside the cilium based on their round-trip journey from the basal body to the tip and back again (Eq. 20).

cilia (or slower-beating cilia) will lengthen because the lowered coupling force will indicate a shorter cilium, and 3) motile cells with longer flagella will beat more slowly. Minoura and Kamiya (55) presented data indicating that prediction 1 may be true in *Chlamydomonas* cells (where the structure that is homologous to a cilium is called a flagellum), i.e., increasing viscosity causes a decrease in angular velocity. This effect was particularly notable in two inner dynein arm mutants (*ida1* and *ida4*). In wild-type cells, though, doubling the viscosity led to only an ~20% decrease in angular velocity. However, the cell could use a length change of ~2 μm to offset the rest of the viscosity change. To test for this length change, we repeated Minoura and Kamiya's experiment with wild-type CC125 cells at 1 cP (normal viscosity of media) and 2 cP (double viscosity) grown in TAP media (prepared with methylcellulose 4000) for 24 h. Although the swim speed was visibly reduced in the 2 cP media, the cells maintained the same mean flagellar length (Student's two-tailed t-test, $p < 0.97$, $N = 50$ for each treatment, mean length ~12.5 μm), casting doubt on the model. Minoura and Kamiya noted a difference in the viscosity response of live cells versus detergent-killed cells that swim when incubated in an ATP buffer. They suggested that live cells sense the viscosity of their media. Although this may be true, cells do not appear to use significant flagellar length changes to offset changes in the fluid couple.

TABLE 2 Model selection with Akaike's information criterion

Model	Parameters	RSS	AIC	ΔAIC	Likelihood	Probability (%)
AIC for IFT Rate Data						
Constant injection	1	72,872	1112.6	85.3	3.00 E-19	9.99 E-18
Initial bolus	2	45,566	1027.3	0	1.0	33.3
Swim speed	3	47,507	1037.1	9.8	7.45 E-03	0.248
Time of flight	4	44,697	1027.9	0.6	0.741	24.6
Ciliary current	2	45,566	1002.5	0	1.0	33.3
Linear diffusion	4	45,566	1031.4	4.10	0.129	4.28
Volumetric diffusion	4	45,566	1031.4	4.10	0.129	4.28
				sum:	3.01	100
AIC for Basal Body Accumulation Data						
Constant injection	1	12,987	1180.4	93.7	4.50 E-21	1.94 E-19
Initial bolus	2	9645.0	1086.7	0	1.0	43.1
Swim speed	3	10,421	1113.3	26.6	1.67 E-06	7.21 E-07
Time of flight	4	9688.0	1092.2	5.50	0.0639	2.75
Ciliary current	2	9645.0	1086.7	0	1.0	43.1
Linear diffusion	4	9645.0	1090.8	4.10	0.129	5.55
Volumetric diffusion	4	9645.0	1090.8	4.10	0.129	5.55
				sum:	2.32	100

To test prediction 2, we obtained length histograms of *Chlamydomonas* paralyzed mutants (Fig. 4). Although most paralyzed mutants have somewhat shorter flagella than wild-type cells, contradicting the swim-speed model, *pf26* mutants are often longer than the wild-type. The PF26 gene encodes a radial spoke protein and thus could be involved in producing the flagellar force (56). However, the fact that the five other *pf* mutants tested showed shorter lengths than the wild-type cells makes it seem more likely that *pf26* has longer flagella for an unrelated reason. Thus, the swim-speed model appears to be an unlikely candidate for flagellar length regulation. We tested prediction 3 by measuring the beat frequency in cilia of wild-type CC125 *Chlamydomonas* cells as well as *lf1* mutant cells, which have longer flagella than the wild-type cells. The *lf1* cells had the same beat frequency as the wild-type cells when the cells had the same lengths of flagella; therefore, we merged the two data sets. In agreement with the swim-speed model, there was a decrease in beat frequency for longer flagellar lengths (Fig. 5). Equation 4 shows that this decrease in beat frequency for longer flagella

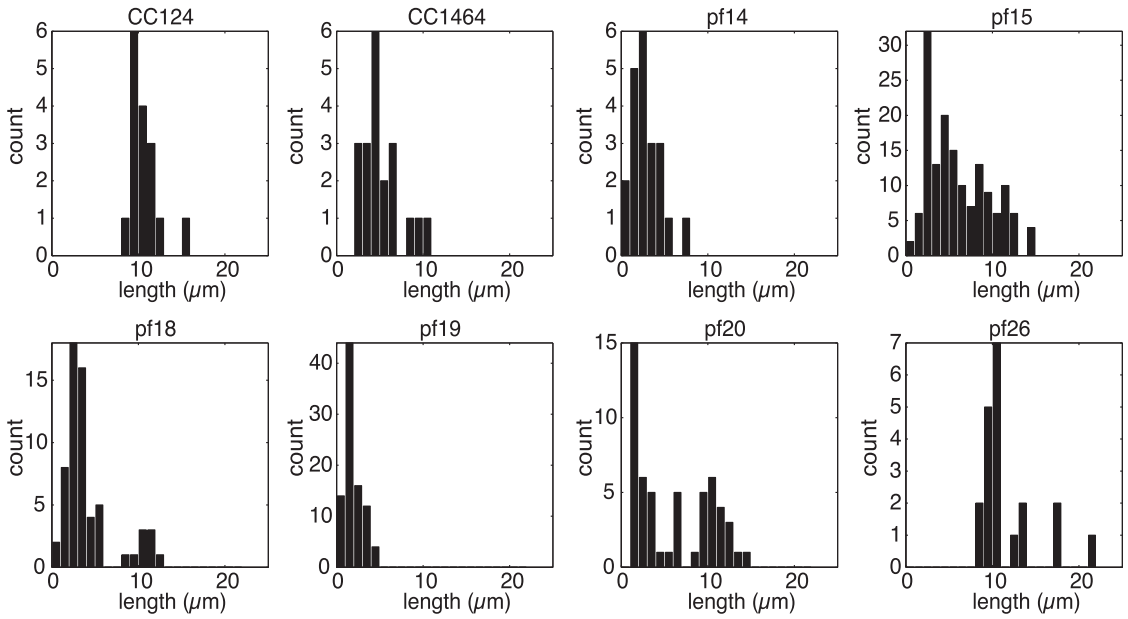

FIGURE 4 Paralyzed flagella (pf) mutants in *Chlamydomonas* display abnormal length distributions. Cells of CC124 (wild-type, $N = 16$), CC1464 (short flagella, $N = 20$), *pf14* ($N = 21$), *pf15* ($N = 153$), *pf18* ($N = 62$), *pf19* ($N = 90$), *pf20* ($N = 54$), and *pf26* ($N = 20$) were measured for flagellar length. Paralyzed flagella from *pf14*, *pf15*, *pf18*, *pf19*, and *pf20* show distributions of decreased length, whereas *pf26* shows some increase in length.

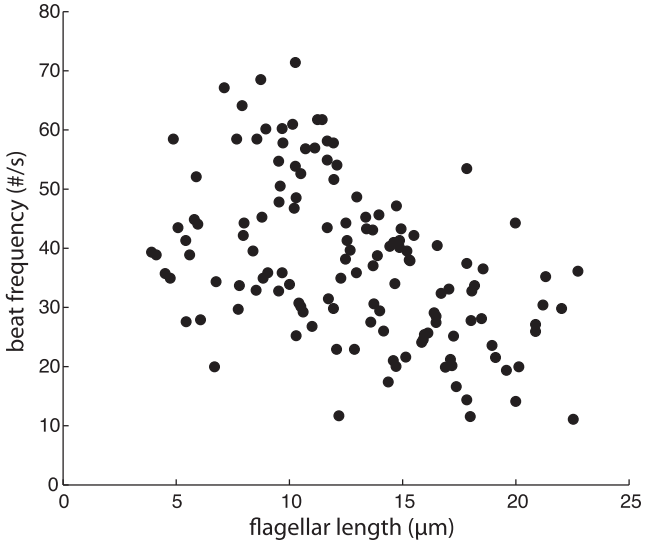

FIGURE 5 Longer flagella beat more slowly. A total of 132 cells of wild-type (CC125) and long-flagella mutant *lf1* were measured for beat frequency (number of beats per second) and flagellar length using a high-speed camera. The decrease in beat frequency for longer flagella offsets some of the length dependence of the swim-speed signal.

will actually offset some of the length dependence of the signal produced by the swim-speed model, making it a poorer measurement of flagellar length.

Model discrimination using live-cell measurements of the IFT rate

Because we have empirically found that the amount of IFT proteins localized to the basal body increases in regenerating flagella of *Chlamydomonas*, we compared each model to the IFT data (Fig. 3). First, we found the best fit of each model's parameters to the data using the NLINFIT function in MATLAB (Fig. 3, *A–G*). Notably, the two diffusion models achieve their best fits with their respective k_2 constants set equal to zero and k_3 constants set equal to one (i.e., the diffusion models perform best when they are algebraically equivalent to the ciliary current and initial bolus models). We then applied the AIC model selection approach (33) to determine which of the IFT control models in Table 1 gives the best fit to two different IFT data sets (see Table 2 for AIC and Fig. 6 for data). The AIC determines the best model by balancing the goodness of fit with the complexity of the model. It weights both the RSS and the number of parameters used by the model. As shown in Table 2, the initial bolus and ciliary ion current models have the highest probability by this analysis across both data sets, followed by the time-of-flight model and the diffusion models.

We note that the two data sets displayed in Fig. 6 represent two distinct ways of quantifying IFT and therefore the two data sets must be fit with different parameters (see the differences in magnitude on the y axes). First, we measured the size and frequency of individual IFT trains by TIRF microscopy in live flagella with a GFP-tagged kinesin II cell line ($N = 186$ flagella; Fig. 6 *A*) (11). Second, we fixed cells and imaged IFT proteins that had accumulated at the basal bodies ($N = 317$; Fig. 6 *B*) (40). This localization appears to control the IFT injection rate and may be directly regulated by the length signal (11).

Differentiating between the initial bolus and ciliary ion current models using FRAP

Although the initial bolus and ciliary ion current models give equivalent mathematical predictions, they give different predictions for photobleaching experiments. Because the initial bolus model proposes that there is no turnover of IFT proteins (i.e., all proteins associated with one flagellum stay with that flagellum for the life of the flagellum), photobleaching GFP-labeled IFT proteins in the cilium should lead to no recovery of fluorescence. To test this prediction, we photobleached KAP-GFP and IFT20-GFP in *Chlamydomonas reinhardtii* flagella using FRAP. Contrary to the initial bolus model, we observed recovery after photobleaching in all cells ($N = 15$), indicating a turnover of IFT components (Fig. 7). We worried that our bleaching may have missed some fluorescence at the basal bodies, allowing recovery from a pool of IFT proteins associated with the basal body of the bleached flagellum. Therefore, we performed additional FRAP experiments in which we bleached more extensively by imaging the flagella long term and photobleaching repeatedly (~10 min of imaging). These experiments yielded similar results: all cells that still had their flagella 5 min after we stopped bleaching recovered flagellar fluorescence ($N = 5$ recovered). Three cells did not recover and instead dropped their flagella, possibly due to photodamage; however, the five cells that were observed to recover their fluorescence could only have done so if the initial bolus model is incorrect and cilia do exchange IFT proteins with the cytoplasmic pool.

The ciliary ion current model gives the best overall fit to IFT data

The data sets have a large amount of scatter (Fig. 6), which could be due to a number of biological or experimental factors. Due to the scatter, and because all of the models fit the data reasonably well by eye (with the exception of the constant injection rate model), model selection alone is not sufficient to rule out any of the models. However, in addition to model selection, many lines of evidence support the ciliary current model. Furthermore, the competing models do a poor job of matching other lines of experimental evidence. Although the initial bolus model and the ciliary current model scored equally well by model selection, the FRAP data rule out the initial bolus model conclusively (Fig. 7).

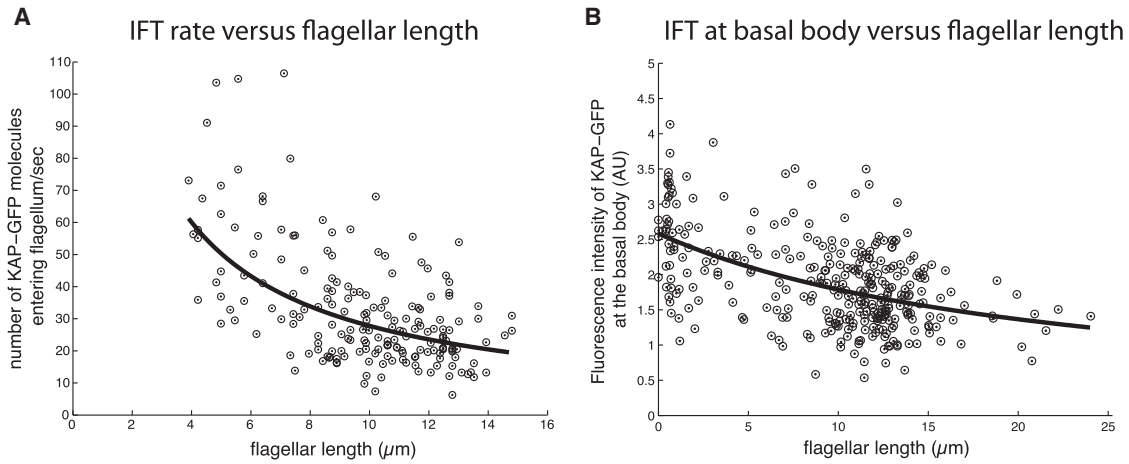

FIGURE 6 (*A* and *B*) IFT decreases as a function of flagellar length for both (*A*) the rate of KAP-GFP injection into the flagellar compartment versus flagellar length ($N = 186$ flagella; see Ludington et al. (11) for methods) and (*B*) basal body accumulation of KAP-GFP protein versus flagellar length data sets ($N = 317$ cells). In (*B*), *Chlamydomonas* cells were deflagellated by pH shock and allowed to regenerate flagella. Aliquots of the regenerating culture were taken at 15 min intervals, fixed, and imaged for GFP fluorescence at the basal body region as previously described (11). The two flagellar lengths per cell were averaged and the two basal bodies were quantified for fluorescence together. The ciliary current model was fit to each data set separately; however, different parameters were calculated for the two fits because the two sets measure different, albeit closely related, processes (see "Placing the models in a ciliary length control context" subsection).

The time-of-flight model also scored well by model selection, but it did a poor job of matching the total flagellar IFT data, which show that the amount of total flagellar IFT remains roughly constant from 1 to 12 μm (16,17).

DISCUSSION

The mechanisms by which a cell can sense the size of its organelles are not known. Here, we have presented mathematical forms of several models, proposed by our group and others, that could determine the length of cilia and allow dynamic regulation of IFT in response to changes in length. To facilitate comparison with experimental measurements, we present the model predictions for the IFT rate, basal body accumulation of IFT proteins, and total injected IFT protein in a flagellum as a function of length. Based on these predictions, we can begin to differentiate between models; however, our results show that further experiments will be necessary to utilize the predictions of these models and to distinguish between models that make similar quantitative predictions. We also note that many of the models are not mutually exclusive (e.g., swim speed may cause additional ciliary ion current) and that combinations of models, such as time of flight delivering signal for linear diffusion, may reasonably be made.

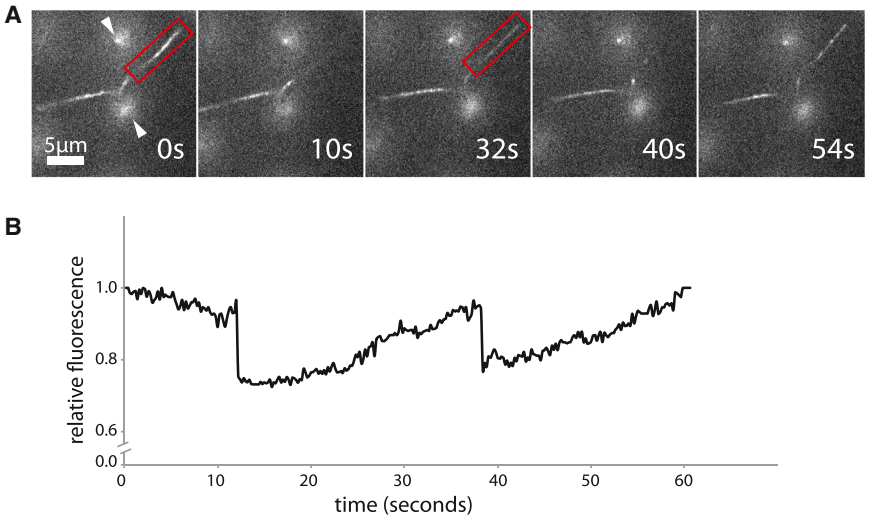

FIGURE 7 The IFT protein shows FRAP. (*A* and *B*) KAP-GFP (KAP) *Chlamydomonas* flagella were bleached (*A*, *red box*) and the total integrated fluorescence in the box was measured over time (*B*, in the *red box*). The fluorescence intensity was normalized to the average integrated fluorescence of the two unbleached cell bodies (*white arrowheads* in the first panel of the montage). IFT20-GFP cells yielded similar results but with faster recovery times. To see this figure in color, go online.

Regulating IFT train cargo loading

A recent study suggested that cargo loading by IFT particles is regulated as a function of length (6). Our models do not speak to this point, as we are modeling the regulation of IFT protein recruitment and injection, which we can directly measure. Clearly, cargo loading could respond to the same length signal that regulates IFT, or to some other sensor mechanism, but the form of the models we present here (e.g., Eq. 19) apply only to the regulation of IFT recruitment and injection.

Possible molecular components of the length-sensing system

These models have been phrased in abstract terms and do not invoke specific molecules. One molecule whose state is known to vary as a function of flagellar length is *Chlamydomonas* aurora-like protein kinase (CALK) (54). Measurements of CALK phosphorylation in *Chlamydomonas* flagella demonstrate that there is a steep change in the sensitivity of the length sensor from 0 to ~6 μm, but that variation in length for longer flagella is not detected (54). Thus, the pattern of phosphorylation empirically observed is similar to the trend seen in the diffusion models: both are highly sensitive to small changes in length at short lengths, but they become less sensitive for lengths $>$ 6 μm. Of interest, though, are the further observations that phosphorylation of CALK on residue T193 tracks flagellar shortening from 12 μm down to ~3 μm (23). Thus, it is possible that multiple length sensors are simultaneously at work to regulate assembly and disassembly separately (15). In any case, modification of CALK is clearly responding to an unknown upstream pathway whose activity is length regulated. Moreover, CALK itself does not seem to play a critical role in length control, since RNAi-mediated knockdown of CALK does not affect steady-state length. Similarly to the CALK data, the finding that CrCDPK1 phosphorylates FLA8 in an assembly-dependent manner (14) implies an upstream length signal that appears to be calcium dependent. Our results agree with these findings and suggest that the length signal may be an inward calcium current in the flagellum.

Testing models with unknown molecular components

Can we test models experimentally without knowing the molecular components of the machinery that senses length? Consider, for example, the time-of-flight model. Clearly, the key experiment would be to identify the signal molecule that is used to measure flagellar/ciliary length; however, an alternative experiment could be used to test the model: if IFT traffic were to be slowed, such as in a temperature-sensitive kinesin at elevated temperature, the flagellum should appear longer to the cell, causing a downregulation of IFT, which might be detected at the basal body. Failure to observe such a response to slowing of IFT would allow us to invalidate the time-of-flight model without needing to know the identity of any of its molecular components. The strong performance of the time-of-flight model in the model selection analysis suggests that this experiment should be done.

In this study, we focused on comparing model predictions with experimental measurements of IFT injection or recruitment as a function of flagellar length. These are not the only data that could in principle be used to evaluate model predictions. In addition to measurements of IFT, measurements of flagellar length as a function of time during flagellar regeneration, which can be used to derive the flagellar growth rate as a function of length, are available. Therefore, it may be possible to test the above models by asking what predictions they make regarding flagellar growth rate versus length. The main concern with such an approach is that to model the length dynamics, as opposed to just modeling IFT injection as we have done, we would require a model for how IFT injection relates to the growth of the flagellum. Given recent results indicating that IFT cargo loading may vary as a function of length (6), such a model would need to be more complex than the simple first-order binding of a constant-concentration precursor pool that we previously invoked (16). Moreover, because flagella are dynamic structures (16,17), their net rate of growth depends on the difference in assembly and disassembly rates, so we would also need a model for how disassembly might vary as a function of length. In contrast to our earlier analysis using IFT mutants (16), which indicated that disassembly is length independent, more recent data indicate that disassembly may also be a function of length (15). Adding these additional length dependencies for disassembly and cargo loading would greatly increase the number of parameters in all of our models. Since we cannot at present directly measure the disassembly and cargo loading dependencies, these parameters would all be hidden, and thus every model would be augmented by multiple free parameters. Therefore, it is unclear whether experimental data on flagellar regeneration would be able to provide any meaningful discrimination if so many additional parameters were to be added to each model.

Can long-zero experiments differentiate between models?

Another existing method that in principle could be used for model discrimination is to measure flagellar length equalization after the severing of one flagella (12,57). In this approach, one flagellum is severed and the length dynamics of the severed and unsevered flagella are measured as the two flagella gradually adjust their lengths to become equal. This experiment provides a rich source of information, but

a direct quantitative comparison with the models presented here would suffer from the same limitations as the flagellar regeneration approach, i.e., the need to add additional parameters to express the unknown length dependencies of cargo loading and flagellar disassembly. However, we can at least ask whether some of our length-sensing models predict the ability of unequal flagellar lengths to equalize. Even if some predict equalization while others do not, this would at least allow us to rule out models that do not give the qualitative prediction that inequalities in length would be equalized. Again, this depends on the assumptions we make about how the assembly rate depends on IFT and how disassembly depends on length. Here, we consider just the simplest assumptions: if we assume that flagellar disassembly is independent of length and that the flagellar assembly rate is proportional to the injection rate of IFT into the cilium, then it can be shown that all of the models in this work will predict equalization of length. This is because for all of the models (other than constant injection), the IFT injection rate is a monotonically decreasing function of length, and hence the net assembly will be a monotonically decreasing function of length. Thus, very short flagella will grow extremely rapidly and thus consume precursor protein from the cytoplasm at a higher rate than at steady state, which in turn will force the long flagellum to shorten (more details about this type of model can be found in Ludington et al. (12)). Thus, with the exception of constant injection, which we have already ruled out based on direct measurements, all of the models are at least qualitatively consistent with the observation of length equalization.

Relating the models to actin-based stereocilia

Stereocilia, actin-based projections with a similar morphology to the tubulin-based cilia discussed here, share many features of growth and maintenance. Although the molecular details are entirely different, both structures grow from their distal tip, are structurally composed of long bundles of cytoskeletal paracrystals, and are maintained by motor traffic moving along the structural bundles from the cytoplasm (58). However, these two types of cilia display three key differences: 1) the growth rate decreases in longer tubulin cilia (16), whereas it increases in longer stereocilia (58); 2) turnover occurs by an unknown mechanism at the tip of tubulin cilia (16), whereas in the stereocilium disassembly it occurs through treadmilling actin, leaving the structure through the proximal base of the organelle (58); and 3) tubulin ciliary assembly appears to be regulated by the base of the organelle (6,11), whereas stereocilia assembly appears to be regulated at the tip (58). Thus, although the molecular details and certain phenomenological aspects of these organelle size-control systems are completely distinct, the overall modeling approach whereby a balance point between assembly and disassembly is achieved is the same for both systems (59). The major distinction between the modeling challenges is that although the length of stereocilia appears to be regulated by inherent transport-based processes, a variety of new findings in tubulin cilia indicate that the ciliary length feeds back on the assembly rate (6,11,13,14).

The ion current model

With respect to the flagellar membrane ion current model, there is good evidence that the flagellar current amplitude correlates with flagellar length when cells are stimulated with a light flash (22). The combination of model selection and FRAP experiments that we present here strongly supports the ciliary calcium current as a length-measuring feedback on IFT. Specifically, in our model, the ion current serves to inhibit IFT. Besschetnova et al.'s (26) results in mammalian cilia provide good evidence for such a scenario. However, previous results obtained by Nultsch et al. (60) using calcium channel blockers on *Chlamydomonas* are puzzling. The ciliary current model predicts that calcium channel blockers should cause ciliary elongation. However, Nultsch et al. detected no such elongation. A more careful revisiting of their experiments and an expansion to other types of channels (e.g., chloride channels) may clarify the previous work. We find the ciliary current model additionally appealing because it can be generalized to measure volume in membrane-bound organelles that are not linear. We can relax specific assumptions of organelle geometry in our derivation, so to measure the volume of any membrane-bound body, such as a lysosome, a golgi body, or the cytoplasm, the model requires only a channel that can read out the membrane potential between the inside and outside of the membrane.

Diffusion-based models

The volume diffusion model as a length sensor also has a tidy mathematical form, with no infinite limits or other unrealistic terms. The model also has few parameters and shows a good fit to the available data sets (Table 2). In cellular terms, it requires only the production of a signal molecule in the flagellum at a constant rate, a flagellar compartment that is separate from the cytoplasm, and degradation of the signal in the cytoplasm (Fig. 1). This scenario resembles that of the RanGTP gradient that regulates nuclear import. Ran, a GTPase, is converted to its excited state in the nucleus by RCC1, the Ran guanine nucleotide exchange factor (RanGEF), and exits the nucleus, where it degrades in the cytoplasm to RanGDP (52). The volume diffusion model proposes a similar scenario that agrees with data and intuition, and resembles an already proven system. The mathematical form of the model could be derived in several ways, yielding slightly different slopes to the predicted curves. Here, we specify

that the ciliary length is sensed as the concentration in the ciliary compartment, but in practice it could be sensed in a variety of ways, including the concentration difference between the cilium and the cytoplasm, or the flux into the cytoplasm. Another part of the derivation that can be changed is how the signal is produced and how it degrades. Regardless of the specific assumptions that are made, the overall trends of the model do not vary under these different derivations. The basic rule—that as the volume of the organelle increases, its concentration of signal decreases—holds true under many different assumptions. Thus, although RCC1 has not been detected in cilia, the biophysical principles of the model are general and may be at work through a different signal molecule or in other organelle compartments. Diffusion is a very general and relevant process that occurs throughout cells. The models presented here show that it can measure the size of membrane-bound compartments.

Diffusion versus intraflagellar transport

Diffusion may also play a role in ciliary assembly in addition to the length-measuring roles proposed here. Levy (32) proposed that diffusion regulates ciliary length before IFT was known to exist (albeit with the questionable assumption that components leak from the tip at a considerable rate). Although there is now overwhelming evidence that IFT delivers ciliary precursors to the tip (4–8) and that diffusion barriers in the ciliary pore and membrane limit the entry of certain proteins (9,61), the flux of tubulin required for ciliary growth is large. At its fastest rate of growth, a cilium can add as much as 0.4 μm of length per minute (49), which requires roughly 10,000 tubulin dimers per minute (8 nm dimer length and ~200 dimers in a cross section of a 9 + 2 motile cilium). And twice that many dimers would be needed per minute if disassembly were to occur simultaneously (12). Assuming that just 10,000 dimers are transported per minute and that ~100 IFT trains travel to the ciliary tip per minute, then each train must haul 100 tubulin dimers in addition to the radial spokes, inner and outer dynein arms, and other core components of the cilium structure—a bulky load. Although it is known that IFT hauls tubulin to the tip (7,8), it is not known whether some tubulin reaches the tip by diffusion. A tubulin dimer's diffusion coefficient is on the order of 10 $\mu m^2/s$, which gives it a Peclet number ($Pe = Lv/D$, where L is the length scale, v is the advection speed, and D is the diffusion coefficient) of ~2 in a 10-μm-long flagellum, assuming an IFT speed of 2 μm/s. Thus, advection (i.e., IFT) is dominant over diffusion, but not by much. When the flagellum is ~1 μm long, Pe is 0.2 and diffusion dominates over advection. Therefore, for a short, regenerating flagellum, diffusion could potentially aid in delivering tubulin to the tip. For larger structural proteins such as radial spokes, the diffusion coefficient is roughly half as large, doubling the Peclet number, and making IFT more important for delivering such cargo to the ciliary tip for assembly. Thus, diffusion may increase the assembly rate in rapidly growing cilia.

Relating the ion current model and diffusion models

The ciliary current and volumetric diffusion models share many aspects, particularly in terms of how the signal can be sensed (the flux of signal molecule into the cytoplasm). The main difference between the models is the source of the signal molecule. In the ciliary current model, the signal is an ion that diffuses into the cilium from the extracellular environment through a membrane channel. This means that length control should be sensitive to the composition of the extracellular medium, which has been shown experimentally for *Chlamydomonas* (46–48). In the volumetric diffusion model, the signal molecule is enzymatically produced inside the cilium. Although RCC1 has not been found inside cilia, other signal molecules could exist for other organelles, and clearly the cell could sense nuclear volume with the RanGTP gradient.

On a final note, both the ciliary current model and the volume diffusion model have the additional appeal of being more general organelle measurement mechanisms. Specific molecules aside, either producing a signal molecule in a compartment or letting one diffuse in from another compartment provide general biophysical principles by which an organelle's size can be determined. Rather than measuring length specifically, they measure organelle volume. In the case of a linear organelle like the cilium, length is proportional to volume, but the models could equally measure an organelle like the nucleus, a vacuole, or the irregularly shaped endoplasmic reticulum. The generality of the models thus gives them potential for broad application and invite testing from outside the field of cilia.

CONCLUSIONS

By formalizing several conceptual models for length sensing in cilia and flagella, we are able to produce mathematical models that make distinct predictions about the relation between length and IFT injection and recruitment to basal bodies. Comparing these predictions with experimental measurements, we find that only a few of the original conceptual models fit the observed data. Taking into account direct photobleaching experiments that rule out the initial bolus model, our results best support the ciliary current and volumetric diffusion models. These results demonstrate our ability to combine simple formal models with quantitative live-cell measurements to narrow down the range of possible conceptual models, and we propose that a similar approach can be used to probe size-control mechanisms for other biological structures.

SUPPORTING MATERIAL

Supporting Materials and Methods and one table are available at http://www.biophysj.org/biophysj/supplemental/S0006-3495(15)00059-4.

ACKNOWLEDGMENTS

We thank Ahmet Yildiz for helpful discussion and Rose Citron for preliminary experiments. We also thank the anonymous reviewers who greatly improved the article.

This work was supported by NIH grant R01 GM097017 to W.M. and NSF-GRFP grants to W.L. and E.K.

REFERENCES

1. Chan, Y. H. M., and W. F. Marshall. 2012. How cells know the size of their organelles. *Science.* 337:1186–1189.
2. Alberts, B., A. D. Johnson, …, P. Walter. 2002. Molecular Biology of the Cell. Garland Science, New York.
3. Marshall, W. F. 2004. Cellular length control systems. *Annu. Rev. Cell Dev. Biol.* 20:677–693.
4. Qin, H., D. T. Burnette, …, J. L. Rosenbaum. 2005. Intraflagellar transport is required for the vectorial movement of TRPV channels in the ciliary membrane. *Curr. Biol.* 15:1695–1699.
5. Cole, D. G., D. R. Diener, …, J. L. Rosenbaum. 1998. Chlamydomonas kinesin-II-dependent intraflagellar transport (IFT): IFT particles contain proteins required for ciliary assembly in Caenorhabditis elegans sensory neurons. *J. Cell Biol.* 141:993–1008.
6. Wren, K. N., J. M. Craft, D. Tritschler, A. Schauer, D. K. Patel, E. F. Smith, M. E. Porter, P. Kner, and K. F. Lechtreck. 2013. A differential cargo-loading model of ciliary length regulation by IFT. *Curr. Biol.* 23:2463–2471.
7. Bhogaraju, S., L. Cajanek, …, E. Lorentzen. 2013. Molecular basis of tubulin transport within the cilium by IFT74 and IFT81. *Science.* 341:1009–1012.
8. Hao, L., M. Thein, …, J. M. Scholey. 2011. Intraflagellar transport delivers tubulin isotypes to sensory cilium middle and distal segments. *Nat. Cell Biol.* 13:790–798.
9. Dishinger, J. F., H. L. Kee, …, K. J. Verhey. 2010. Ciliary entry of the kinesin-2 motor KIF17 is regulated by importin-beta2 and RanGTP. *Nat. Cell Biol.* 12:703–710.
10. Deane, J. A., D. G. Cole, …, J. L. Rosenbaum. 2001. Localization of intraflagellar transport protein IFT52 identifies basal body transitional fibers as the docking site for IFT particles. *Curr. Biol.* 11:1586–1590.
11. Ludington, W. B., K. A. Wemmer, …, W. F. Marshall. 2013. Avalanche-like behavior in ciliary import. *Proc. Natl. Acad. Sci. USA.* 110:3925–3930.
12. Ludington, W. B., L. Z. Shi, …, W. F. Marshall. 2012. Organelle size equalization by a constitutive process. *Curr. Biol.* 22:2173–2179.
13. Pan, J., and W. J. Snell. 2014. Organelle size: a cilium length signal regulates IFT cargo loading. *Curr. Biol.* 24:R75–R78.
14. Liang, Y., Y. Pang, …, J. Pan. 2014. FLA8/KIF3B phosphorylation regulates kinesin-II interaction with IFT-B to control IFT entry and turnaround. *Dev. Cell.* 30:585–597.
15. Hilton, L. K., K. Gunawardane, J. W. Kim, M. C. Schwarz, and L. M. Quarmby. 2013. The kinases LF4 and CNK2 control ciliary length by feedback regulation of assembly and disassembly rates. *Curr. Biol.* 23:2208–2214.
16. Marshall, W. F., and J. L. Rosenbaum. 2001. Intraflagellar transport balances continuous turnover of outer doublet microtubules: implications for flagellar length control. *J. Cell Biol.* 155:405–414.
17. Marshall, W. F., H. Qin, …, J. L. Rosenbaum. 2005. Flagellar length control system: testing a simple model based on intraflagellar transport and turnover. *Mol. Biol. Cell.* 16:270–278.
18. Lefebvre, P. 2009. Flagellar length control. *In* The Chlamydomonas Sourcebook: Cell Motility and Behavior. G. B. Witman, editor. Academic Press, Elsevier, Oxford, pp. 115–129.
19. Pazour, G. J., B. L. Dickert, …, D. G. Cole. 2000. Chlamydomonas IFT88 and its mouse homologue, polycystic kidney disease gene tg737, are required for assembly of cilia and flagella. *J. Cell Biol.* 151:709–718.
20. Rosenbaum, J. 2003. Organelle size regulation: length matters. *Curr. Biol.* 13:R506–R507.
21. Johnson, K. A., and J. L. Rosenbaum. 1993. Flagellar regeneration in Chlamydomonas: a model system for studying organelle assembly. *Trends Cell Biol.* 3:156–161.
22. Beck, C., and R. Uhl. 1994. On the localization of voltage-sensitive calcium channels in the flagella of Chlamydomonas reinhardtii. *J. Cell Biol.* 125:1119–1125.
23. Cao, M., D. Meng, …, J. Pan. 2013. Activation loop phosphorylation of a protein kinase is a molecular marker of organelle size that dynamically reports flagellar length. *Proc. Natl. Acad. Sci. USA.* 110:12337–12342.
24. Praetorius, H. A., J. Frokiaer, …, K. R. Spring. 2003. Bending the primary cilium opens Ca^{2+}-sensitive intermediate-conductance K^{+} channels in MDCK cells. *J. Membr. Biol.* 191:193–200.
25. Praetorius, H. A., and K. R. Spring. 2001. Bending the MDCK cell primary cilium increases intracellular calcium. *J. Membr. Biol.* 184: 71–79.
26. Besschetnova, T. Y., E. Kolpakova-Hart, …, J. V. Shah. 2010. Identification of signaling pathways regulating primary cilium length and flow-mediated adaptation. *Curr. Biol.* 20:182–187.
27. Abdul-Majeed, S., and S. M. Nauli. 2011. Calcium-mediated mechanisms of cystic expansion. *Biochim. Biophys. Acta.* 1812:1281–1290.
28. Osterman, N., and A. Vilfan. 2011. Finding the ciliary beating pattern with optimal efficiency. *Proc. Natl. Acad. Sci. USA.* 108:15727–15732.
29. Tam, D., and A. E. Hosoi. 2011. Optimal feeding and swimming gaits of biflagellated organisms. *Proc. Natl. Acad. Sci. USA.* 108:1001–1006.
30. Brennen, C., and H. Winet. 1977. Fluid mechanics of propulsion by cilia and flagella. *Annu. Rev. Fluid Mech.* 9:339–398.
31. Harris, J. E. 1961. The mechanics of ciliary movement. *In* The Cell and the Organism. J. A. Ramsay and V. B. Wigglesworth, editors. Cambridge University Press, London/New York, pp. 22–36.
32. Levy, E. M. 1974. Flagellar elongation as a moving boundary problem. *Bull. Math. Biol.* 36:265–273.
33. Akaike, H. 1974. A new look at the statistical model identification. *IEEE Trans. Automat. Contr.* 19:716–723.
34. Burnham, K., and D. Anderson. 2004. Multimodel inference: understanding AIC and BIC in model selection. *Sociol. Methods Res.* 33:261.
35. Ludington, W., and W. Marshall. 2009. Automated analysis of intracellular motion using kymographs in 1, 2, and 3 dimensions. *Proc. SPIE.* 7184:32.
36. Mueller, J., C. A. Perrone, …, M. E. Porter. 2005. The FLA3 KAP subunit is required for localization of kinesin-2 to the site of flagellar assembly and processive anterograde intraflagellar transport. *Mol. Biol. Cell.* 16:1341–1354.
37. Lechtreck, K.-F., E. C. Johnson, …, G. B. Witman. 2009. The Chlamydomonas reinhardtii BBSome is an IFT cargo required for export of specific signaling proteins from flagella. *J. Cell Biol.* 187:1117–1132.
38. Pazour, G. J., N. Agrin, …, G. B. Witman. 2005. Proteomic analysis of a eukaryotic cilium. *J. Cell Biol.* 170:103–113.
39. Stolc, V., M. P. Samanta, …, W. F. Marshall. 2005. Genome-wide transcriptional analysis of flagellar regeneration in Chlamydomonas reinhardtii identifies orthologs of ciliary disease genes. *Proc. Natl. Acad. Sci. USA.* 102:3703–3707.

40. Avasthi, P., M. Onishi, J. Karpiak, R. Yamamoto, L. Mackinder, M. C. Jonikas, W. S. Sale, B. Shoichet, J. R. Pringle, and W. F. Marshall. 2014. Actin is required for IFT regulation in Chlamydomonas reinhardtii. *Curr. Biol.* 24:2025–2032.

41. Makishima, S., K. Komoriya, …, S. I. Aizawa. 2001. Length of the flagellar hook and the capacity of the type III export apparatus. *Science.* 291:2411–2413.

42. Jeffery, G. B. 1922. The motion of ellipsoidal particles immersed in a viscous fluid. *Proc. R. Soc. Lond. A Math. Phys. Sci.* 102:161–179.

43. Engel, B. D., W. B. Ludington, and W. F. Marshall. 2009. Intraflagellar transport particle size scales inversely with flagellar length: revisiting the balance-point length control model. *J. Cell Biol.* 187:81–89.

44. Witman, G. B. 1993. Chlamydomonas phototaxis. *Trends Cell Biol.* 3:403–408.

45. Patel, A. 2014. The primary cilium calcium channels and their role in flow sensing. *Pflügers Arch.* 467:157–165.

46. Solter, K. M., and A. Gibor. 1978. The relationship between tonicity and flagellar length. *Nature.* 275:651–652.

47. Telser, A. 1977. The inhibition of flagellar regeneration in Chlamydomonas reinhardii by inhalational anesthetic halothane. *Exp. Cell Res.* 107:247–252.

48. Bloodgood, R. A., E. M. Leffler, and A. T. Bojczuk. 1979. Reversible inhibition of Chlamydomonas flagellar surface motility. *J. Cell Biol.* 82:664–674.

49. Lefebvre, P. A., S. A. Nordstrom, …, J. L. Rosenbaum. 1978. Flagellar elongation and shortening in Chlamydomonas. IV. Effects of flagellar detachment, regeneration, and resorption on the induction of flagellar protein synthesis. *J. Cell Biol.* 78:8–27.

50. Abu-Arish, A., P. Kalab, …, C. Fradin. 2009. Spatial distribution and mobility of the Ran GTPase in live interphase cells. *Biophys. J.* 97:2164–2178.

51. Kalab, P., and R. Heald. 2008. The RanGTP gradient—a GPS for the mitotic spindle. *J. Cell Sci.* 121:1577–1586.

52. Becskei, A., and I. W. Mattaj. 2003. The strategy for coupling the RanGTP gradient to nuclear protein export. *Proc. Natl. Acad. Sci. USA.* 100:1717–1722.

53. Liang, Y., and J. Pan. 2013. Regulation of flagellar biogenesis by a calcium dependent protein kinase in Chlamydomonas reinhardtii. *PLoS ONE.* 8:e69902.

54. Luo, M., M. Cao, …, J. Pan. 2011. The phosphorylation state of an aurora-like kinase marks the length of growing flagella in Chlamydomonas. *Curr. Biol.* 21:586–591.

55. Minoura, I., and R. Kamiya. 1995. Strikingly different propulsive forces generated by different dynein-deficient mutants in viscous media. *Cell Motil. Cytoskeleton.* 31:130–139.

56. Lefebvre, P. A., and J. L. Rosenbaum. 1986. Regulation of the synthesis and assembly of ciliary and flagellar proteins during regeneration. *Annu. Rev. Cell Biol.* 2:517–546.

57. Rosenbaum, J. L., J. E. Moulder, and D. L. Ringo. 1969. Flagellar elongation and shortening in Chlamydomonas. The use of cycloheximide and colchicine to study the synthesis and assembly of flagellar proteins. *J. Cell Biol.* 41:600–619.

58. Rzadzinska, A. K., M. E. Schneider, …, B. Kachar. 2004. An actin molecular treadmill and myosins maintain stereocilia functional architecture and self-renewal. *J. Cell Biol.* 164:887–897.

59. Prost, J., C. Barbetta, and J.-F. Joanny. 2007. Dynamical control of the shape and size of stereocilia and microvilli. *Biophys. J.* 93:1124–1133.

60. Nultsch, W., J. Pfau, and R. Dolle. 1986. Effects of calcium channel blockers on phototaxis and motility of Chlamydomonas reinhardtii. *Arch. Microbiol.* 144:393–397.

61. Hu, Q., L. Milenkovic, …, W. J. Nelson. 2010. A septin diffusion barrier at the base of the primary cilium maintains ciliary membrane protein distribution. *Science.* 329:436–439.